

OPTIMIZING TALBOT'S CONTOURS FOR THE INVERSION OF THE LAPLACE TRANSFORM*

J. A. C. WEIDEMAN†

Abstract. Talbot's method for the numerical inversion of the Laplace transform consists of numerically integrating the Bromwich integral on a special contour by means of the trapezoidal or midpoint rules. In this paper we address the issue of parameter selection in the method, for the particular situation when parabolic PDEs are solved. In the process the well-known subgeometric convergence rate $O(\exp(-c\sqrt{N}))$ of this method is improved to the geometric rate $O(\exp(-cN))$, with N the number of nodes in the integration rule. The value of the maximum decay rate c is explicitly determined. Numerical results for two versions of the heat equation are presented. With the choice of parameters derived here, the rule of thumb is that to achieve an accuracy of $10^{-\ell}$ at any given time, the associated elliptic problem has to be solved no more than ℓ times.

Key words. Laplace transform, Talbot's method, trapezoidal rule, fractional differential equation

AMS subject classifications. 65D30, 65M70, 65R10

DOI. 10.1137/050625837

1. Introduction. The Laplace transform is a classical technique for solving linear differential equations. For computational work, however, this approach never really became popular, as for many years numerical analysts tended to focus on discretization methods such as finite differences and finite elements, possibly combined with linear multistep or Runge–Kutta formulas for integration in time. We conjecture that this lack of interest shown by numerical analysts in the Laplace transform is partly due to the following two factors.

First, the Laplace transform restricts one to linear differential equations and in many applications one ultimately aims to solve nonlinear problems. Second, the Laplace transform, particularly its numerical inversion, has a reputation for being a computational challenge. This has to do with the fact that the inverse problem is by nature ill-conditioned when the transform is known only as a real-valued function. When the transform can be sampled in the complex plane the conditioning seems better, but then complex arithmetic is required.

Despite these apparent drawbacks of the Laplace transform, there has been a recent resurgence of the technique, as evidenced by the number of papers on this topic that have appeared since the year 2000; see, for example, [4, 8, 12, 14, 17, 18]. This renewed activity is in part due to recent interest in linear parabolic PDEs of fractional type, which are naturally posed in a transform setting. (These fractional PDEs model phenomena such as anomalous diffusion in several financial and biological applications.) In addition, MATLAB and other modern computational environments make complex arithmetic as easy to work with as real arithmetic and therefore complex inversion formulas become feasible.

*Received by the editors March 3, 2005; accepted for publication (in revised form) June 9, 2006; published electronically November 24, 2006. This work was supported by the National Research Foundation in South Africa under grant FA2005032300018.

<http://www.siam.org/journals/sinum/44-6/62583.html>

†Department of Applied Mathematics, University of Stellenbosch, Private Bag X1, Matieland 7602, South Africa (weideman@dip.sun.ac.za). This work was done at the Oxford University Computing Laboratory, as Visiting Fellow of Exeter College, Oxford, while the author was on sabbatical leave from the University of Stellenbosch, South Africa.

To introduce the problem, consider the linear system of ODEs

$$(1.1) \quad \frac{d\mathbf{f}}{dt} = A\mathbf{f}, \quad \mathbf{f}(0) = \mathbf{f}_0,$$

where A is an $M \times M$ real matrix, $\mathbf{f}(t)$ an $M \times 1$ real vector, and \mathbf{f}_0 the initial condition. We are primarily interested in the case where A is the result of semi-discretization of a parabolic PDE (examples are given in section 5). We assume, therefore, that the eigenvalues of A are real and negative.

The formal solution to (1.1) is

$$\mathbf{f}(t) = \exp(At) \mathbf{f}_0,$$

and this reduces the problem to that of computing the matrix exponential of a (typically) large matrix. To be more precise, we need to compute the product of the matrix exponential and a vector, which can be done without actually computing the matrix exponential itself [15].

The authors of [4, 8, 12, 14, 17, 18] all compute this product by numerically approximating the inverse Laplace transform

$$(1.2) \quad \mathbf{f}(t) = \frac{1}{2\pi i} \int_{\Gamma} e^{zt} \mathbf{F}(z) dz, \quad \mathbf{F}(z) \equiv (zI - A)^{-1} \mathbf{f}_0.$$

In this formula, known as the Bromwich integral, I is the $M \times M$ identity matrix and Γ is the contour of integration. At least initially, Γ is the Bromwich line $\operatorname{Re} z = \sigma$, where the parameter σ should be large enough that all eigenvalues of A lie in the half-plane $\operatorname{Re} z < \sigma$.

The typical approach is to deform the Bromwich line into a curve that begins and ends in the left half-plane, such that $\operatorname{Re} z \rightarrow -\infty$ on the contour; see Figure 1.1. Owing to the exponential factor e^{zt} , the integrand decays rapidly on such a contour, and if the contour is smooth this turns the problem into one of the classic situations where the trapezoidal rule converges extraordinarily rapidly [5, 10, 22, 23].

The articles [4, 8, 12, 14, 17, 18] differ with respect to the choice of the integration contour Γ , and how this contour is parameterized. A short summary of contours and convergence rates is given in section 6.

Surprisingly, none of the above references seriously considers Talbot's contour [19], rated in some circles as one of the best methods for inverting the Laplace transform; see [6]. (The method is mentioned in [12, 18], but is neither implemented nor analyzed there.) This contour may not be suitable when part of the spectrum of A is located off the negative real axis, but for pure parabolic problems the method is very accurate, as the numerical results of this paper will testify.

Talbot's contour is parameterized by

$$(1.3) \quad \Gamma: \quad z(\theta) = \sigma + \mu(\theta \cot \theta + \nu i \theta), \quad -\pi \leq \theta \leq \pi,$$

where σ , μ , and ν are real parameters that determine the geometry of the curve. Both μ and ν are positive. For the eigenvalues of A to be enclosed by the contour one needs $z(0) > \lambda$, where λ is the largest eigenvalue of A , i.e.,

$$(1.4) \quad \sigma + \mu > \lambda.$$

A typical Talbot contour is shown in Figure 1.1.

A related contour is obtained by replacing the function $\theta \cot \theta$ in (1.3) with the first two terms in its partial fraction expansion,

$$(1.5) \quad \Gamma: \quad z(\theta) = \sigma + \mu \left(1 + \frac{2\theta^2}{\theta^2 - \pi^2} + \nu i \theta \right), \quad -\pi \leq \theta \leq \pi.$$

This contour is equivalent to one mentioned in Talbot's original paper [19], from which we quote: "...and indeed such functions can give good results, though their potentialities have not yet been explored."

It will turn out that the contour (1.5) is easier to analyze than (1.3), so for much of the paper we shall focus on the second contour. We shall also show, however, that the first Talbot contour yields superior accuracy.

Using either (1.3) or (1.5), the Bromwich integral (1.2) can be expressed as

$$(1.6) \quad \mathbf{f}(t) = \frac{1}{2\pi i} \int_{-\pi}^{\pi} e^{z(\theta)t} \mathbf{F}(z(\theta)) z'(\theta) d\theta,$$

where, respectively,

$$z'(\theta) = \mu (\cot \theta - \theta \csc^2 \theta + \nu i) \quad \text{or} \quad z'(\theta) = \mu \left(-\frac{4\pi^2 \theta}{(\theta^2 - \pi^2)^2} + \nu i \right).$$

The integral (1.6) is typically approximated by the trapezoidal rule on a uniform partition of $[-\pi, \pi]$. Instead, we prefer to use the equally accurate midpoint rule with an even number of intervals, say $2N$. This is a practical choice that avoids sampling the integrand at the removable singularity at $\theta = 0$, as well as at the essential singularities at $\theta = \pm\pi$.

We hence define the grid

$$(1.7) \quad \theta_k = (2k + 1) \frac{\pi}{2N}, \quad k = -N, \dots, N - 1,$$

and denote the approximation to (1.6) by

$$\mathbf{f}_N(t) = \frac{1}{2N i} \sum_{k=-N}^{N-1} e^{z(\theta_k)t} z'(\theta_k) \mathbf{F}_k,$$

or

$$(1.8) \quad \mathbf{f}_N(t) = \frac{1}{N} \operatorname{Im} \left\{ \sum_{k=0}^{N-1} e^{z(\theta_k)t} z'(\theta_k) \mathbf{F}_k \right\},$$

if symmetry is used. Here the vectors $\mathbf{F}_k \equiv \mathbf{F}(z(\theta_k))$ are solved from

$$(1.9) \quad \left(z(\theta_k) I - A \right) \mathbf{F}_k = \mathbf{f}_0, \quad k = 0, \dots, N - 1.$$

Unless A is sparse, the solution of the N linear systems (1.9) represents the bulk of the computational cost of the algorithm. It should, however, be noted that the systems (1.9) can be solved independently and in parallel [10, 17]. In addition, it is possible to solve all N systems (1.9) efficiently using a single Hessenberg or Schur decomposition of A ; see Problem P7.4.2 in [9, p. 350].

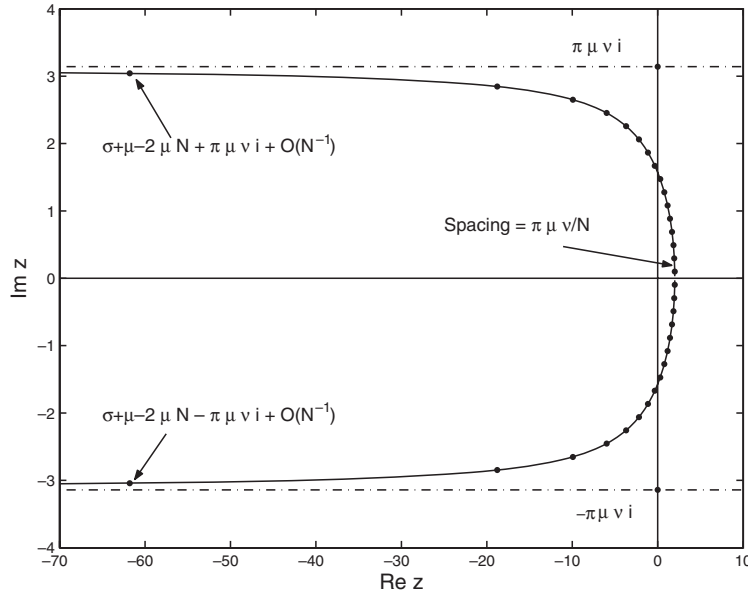


FIG. 1.1. Talbot's contour (1.3) with parameter values $\sigma = 0$, $\mu = 2$, $\nu = 0.5$. The dots are the images in the z -plane of the midpoint abscissas (1.7).

In this paper, we shall aim to optimize the convergence rate $\mathbf{f}_N(t) \rightarrow \mathbf{f}(t)$ as $N \rightarrow \infty$, keeping t fixed, by selecting the parameters (σ, μ, ν) in (1.3) and (1.5) to be asymptotically optimal. This is achieved by making σ and μ both proportional to the ratio N/t . By doing so, a geometric convergence rate, $O(e^{-cN})$ as $N \rightarrow \infty$, can be obtained. It is well known that Talbot's method with fixed (and therefore suboptimal) parameters converges at a subgeometric rate of $O(e^{-c\sqrt{N}})$; see [19].

To conclude this introduction, we offer Figure 1.1 as a summary of the role of the parameters (σ, μ, ν) in the contour (1.3). The parameter σ represents a shift to the left or right. The parameter μ controls the distance that the two extreme nodes extend into the left half-plane. The parameter ν determines the width of the contour in the sense that the contour approaches two horizontal asymptotes at distance proportional to $\mu\nu$ from the real axis as $\text{Re } z \rightarrow -\infty$. The factor $\mu\nu$ also determines the spacing of the nodes near the real axis.

The outline of the paper is as follows. In section 2, we indicate how the well-known $O(e^{-c\sqrt{N}})$ convergence rate can be rederived by analyzing the scalar model problem

$$(1.10) \quad f(t) = e^{\lambda t}, \quad F(z) = (z - \lambda)^{-1}.$$

This analysis suggests the reparameterization that we alluded to above, namely to make σ and μ both proportional to N/t . A saddle point method is used in section 3 to demonstrate that this rescaling of parameters leads to an improved convergence rate $O(e^{-cN})$. In section 4, we determine the value of ν and the proportionality constants in $\sigma \propto N/t$, $\mu \propto N/t$ that will maximize the decay rate, c . We hence obtain the attractive convergence rates $O(e^{-1.90N})$ and $O(e^{-1.73N})$, respectively, for the two versions of the Talbot contour (1.3) and (1.5). A further improvement, which involves omitting those outlying nodes on the Talbot contour that make a negligible

contribution to the midpoint sum, improves these two convergence rates to effectively $O(e^{-2.41N})$ and $O(e^{-2.56N})$. The theory of sections 3 and 4 is tested on two parabolic PDEs in section 5. In section 6, we discuss a few alternate contours, and we also contrast the parameter suggestions of this paper with those made by Talbot in [19].

2. Analysis of the scalar problem. We suppose the matrix A , which may or may not be symmetric, has real and negative eigenvalues, λ_j , corresponding to a complete set of eigenvectors, \mathbf{v}_j , $j = 1, \dots, M$. If one expands the initial condition as a linear combination of eigenvectors,

$$\mathbf{f}_0 = c_1 \mathbf{v}_1 + \dots + c_M \mathbf{v}_M,$$

then (1.2) can be expressed as

$$\mathbf{f}(t) = \frac{c_1}{2\pi i} \left(\int_{\Gamma} \frac{e^{zt}}{z - \lambda_1} dz \right) \mathbf{v}_1 + \dots + \frac{c_M}{2\pi i} \left(\int_{\Gamma} \frac{e^{zt}}{z - \lambda_M} dz \right) \mathbf{v}_M.$$

Applying Talbot’s method to the right-hand side is therefore equivalent to applying it to the scalar problem (1.10), where λ represents a real and negative eigenvalue of A . For any fixed t , we shall restrict attention to λ in the range $|\lambda t| = O(1)$ as $M \rightarrow \infty$. We consider this sufficient because in the actual solution,

$$\mathbf{f}(t) = c_1 e^{\lambda_1 t} \mathbf{v}_1 + \dots + c_M e^{\lambda_M t} \mathbf{v}_M,$$

modes that satisfy $|\lambda t| \gg 1$ are negligible.

Our task is therefore to estimate the error when approximating the integral

$$(2.1) \quad f(t) = \frac{1}{2\pi i} \int_{-\pi}^{\pi} \frac{e^{z(\theta)t}}{z(\theta) - \lambda} z'(\theta) d\theta$$

with the midpoint rule, with $z(\theta)$ defined by (1.3) or (1.5), and $\lambda < 0$. To start, we recall an error formula for the midpoint rule.

Consider an integral on $[-\pi, \pi]$ and its midpoint rule approximation

$$(2.2) \quad I(g) = \int_{-\pi}^{\pi} g(\theta) d\theta, \quad M_N(g) = \frac{\pi}{N} \sum_{k=-N}^{N-1} g(\theta_k),$$

where the nodes θ_k are defined by (1.7). Suppose that the function $g(\theta)$ has an absolutely convergent Fourier series expansion

$$g(\theta) = \sum_{k=-\infty}^{\infty} c_k e^{ik\theta}, \quad \text{with} \quad c_k = \frac{1}{2\pi} \int_{-\pi}^{\pi} g(\theta) e^{-ik\theta} d\theta.$$

Then it is possible to insert these formulas into (2.2), followed by termwise integration and summation, to obtain

$$I(g) = 2\pi c_0, \quad M_N(g) = 2\pi c_0 + 2\pi \sum_{\substack{\ell=-\infty \\ \ell \neq 0}}^{\infty} (-1)^\ell c_{2\ell N}.$$

The error is therefore given by

$$(2.3) \quad I(g) - M_N(g) = -2\pi \sum_{\substack{\ell=-\infty \\ \ell \neq 0}}^{\infty} (-1)^\ell c_{2\ell N}.$$

(The trapezoidal rule error would be similar, except for the absence of the $(-1)^\ell$ factor; see [23].)

When the periodic extension of $g(\theta)$ is infinitely differentiable on $[-\pi, \pi]$, the Fourier coefficients c_k decay rapidly. In fact, repeated integration by parts can then be used to establish $c_k = O(|k|^{-m})$ for each positive integer m . In such cases a good error estimate can be obtained by retaining only the leading two terms in (2.3), as follows:

$$\begin{aligned} I(g) - M_N(g) &\sim 2\pi(c_{-2N} + c_{2N}) \\ &= \int_{-\pi}^{\pi} g(\theta)e^{-2Ni\theta} d\theta + \int_{-\pi}^{\pi} g(\theta)e^{+2Ni\theta} d\theta. \end{aligned}$$

One may apply this estimate to the special integral (2.1). The factor $e^{z(\theta)t}$ decays sufficiently rapidly as $\theta \rightarrow \pm\pi$ to ensure infinite differentiability of the periodic extension of the integrand. We therefore propose to analyze the error estimate,

$$f(t) - f_N(t) \sim E_N^-(t) + E_N^+(t), \quad N \rightarrow \infty,$$

where, using symmetry,

$$(2.4) \quad E_N^\pm(t) = \frac{1}{\pi} \text{Im} \left\{ \int_{-\pi}^0 \frac{e^{z(\theta)t \pm 2iN\theta}}{z(\theta) - \lambda} z'(\theta) d\theta \right\}.$$

We shall keep both $t > 0$ and $\lambda < 0$ fixed, as well as the parameters $\sigma, \mu,$ and ν in the contours (1.3) or (1.5); our interest is the behavior of (2.4) as $N \rightarrow \infty$.

We digress for a moment to point out that error estimates such as (2.4) were used to good effect by Lin, to numerically predict optimal parameters for Talbot's contour [11]. A wide range of transforms was considered there, not just the $F(z) = 1/(z - \lambda)$ considered here.

Rather than using numerical optimization, we shall instead use the saddle point method to estimate analytically the two integrals (2.4). Since this analysis is primarily used to justify the form of the rescaling of parameters in section 3, and not in the determination of the actual optimal numbers itself, we omit the details. (A sketch of the derivation can be found in [24].) The result is that, with $E_N(t) \equiv E_N^-(t) + E_N^+(t)$,

$$(2.5) \quad E_N(t) = O\left(e^{(\sigma+\mu)t-2\sqrt{\pi\mu tN}}\right), \quad N \rightarrow \infty,$$

in the case of contour (1.3), and

$$(2.6) \quad E_N(t) = O\left(e^{(\sigma+\frac{5}{2}\mu)t-2\sqrt{\pi\mu tN}}\right), \quad N \rightarrow \infty,$$

in the case of (1.5). Results similar to these were obtained by Talbot [19, eq. (15)], who used a different method to prove that

$$E_N(t) = O\left(N^2 e^{(\sigma+a\mu)t-b\sqrt{tN}}\right).$$

The constants a and b depend on the transform and the contour.

The factor $5/2$ that appears in (2.6) indicates that the error constant associated with the modified contour (1.5) is larger than that of the original contour (1.3). This was confirmed by the numerical experiments in [24].

The estimates (2.5)–(2.6) suggest the strategy of choosing $\sigma, \mu \propto N/t$. This should improve the subgeometric convergence rate, $O(e^{-c\sqrt{N}})$, to pure geometric convergence, $O(e^{-cN})$. We consider this next.

3. New parameters for the contour. Consider the rescaling

$$(3.1) \quad \sigma = -s \frac{N}{t}, \quad \mu = m \frac{N}{t}, \quad \nu = n,$$

where s , m , and n are real parameters to be determined. Both m and n are positive, and in accordance with (1.4) we require that

$$(3.2) \quad s < m - \frac{\lambda t}{N}.$$

The constant λ is defined in (1.10), which we continue to use as the model problem.

Because the parameters become dependent on t , so does the contour and hence also the integration nodes. This means that the N linear systems (1.9) have to be solved for each value of t , which may be inefficient. We therefore intend this rescaling to be used when the solution is required at only a few values of t .

Using the new parameters (3.1) we define $\zeta(\theta) = (t/N) z(\theta)$; i.e.,

$$(3.3) \quad \zeta(\theta) = -s + m \left(\theta \cot \theta + i n \theta \right)$$

in the case of the contour (1.3), and

$$(3.4) \quad \zeta(\theta) = -s + m \left(1 + \frac{2\theta^2}{\theta^2 - \pi^2} + i n \theta \right)$$

in the case of (1.5). The two error integrals (2.4) therefore become

$$(3.5) \quad E_N^\pm(t) = \frac{1}{\pi} \operatorname{Im} \left\{ \int_{-\pi}^0 \frac{e^{N g_\pm(\theta)}}{\zeta(\theta) - \lambda t/N} \zeta'(\theta) d\theta \right\},$$

where

$$g_\pm(\theta) = \zeta(\theta) \pm 2i\theta.$$

We apply the saddle point method to (3.5). (For details of this method, we refer the reader to [1, sect. 6.4; 3, sect. 6.6].) The idea is to deform the interval of integration, $[-\pi, 0]$, to a special contour in the complex θ -plane on which the integral can be estimated accurately. By Cauchy's theorem such a deformed contour will be permissible as long as it starts at $\theta = -\pi$, terminates at $\theta = 0$, and does not cross any singularities of the integrand in between. Suitable contours are steepest descent curves, defined by $\operatorname{Im}\{g_\pm(\theta)\} = \text{constant}$, for these remove the oscillations from the integrands in (3.5). The constants are chosen such that the contours pass through the saddle points, $\theta = \theta_+$ and $\theta = \theta_-$, respectively, defined by

$$(3.6) \quad g'_+(\theta) = 0, \quad g'_-(\theta) = 0.$$

To ensure analyticity of the integrand, one needs to take into consideration the singularities associated with the vanishing of the denominator in (3.5), i.e., the zeros of $\zeta(\theta) = \lambda t/N$. In view of the discussion in the first paragraph of section 2, we shall assume $|\lambda t| \ll N$ and ignore the right-hand side of this equation. We therefore define the critical points, $\theta = \theta_*$, as the zeros of

$$(3.7) \quad \zeta(\theta) = 0.$$

This is the same as setting $\lambda = 0$, and in accordance with (3.2) we shall therefore consider only $m > s$.

To apply the saddle point method, we have to know where the critical points and saddle points are. We restrict ourselves to the modified contour (1.5); i.e., we assume $\zeta(\theta)$ is defined by (3.4). For this contour (3.6) and (3.7) reduce to polynomial equations of degrees 4 and 3, respectively, which can in principle be solved explicitly. The results are unwieldy, however, and we follow a more elementary approach.

In order to work with equations with real coefficients, we introduce the variable ϕ by $\theta = i\phi$. After denominators have been cleared, (3.6) can be factored into

$$(3.8) \quad (mn \pm 2)(\phi^2 + \pi^2)^2 = 4m\pi^2\phi,$$

and (3.7) into

$$(3.9) \quad (mn\phi + s - m)(\phi^2 + \pi^2) = 2m\phi^2.$$

Assuming $m > s \geq 0$ and working with these two representations, we were able to establish the following properties of the roots of (3.6)–(3.7).

Starting with the cubic equation (3.9), it is readily established that it always has a positive real root. The remaining two roots may either be real as well or occur as a conjugate pair. In the latter case the real part of these roots is positive, and the imaginary part is bounded in absolute value by π . Transplanting this information from the ϕ variable to θ , we deduce that the three critical points θ_* defined by (3.7) are all in the upper half-plane, with real parts in the interval $(-\pi, \pi)$. At least one root lies on the positive imaginary axis. The other two roots may be pure imaginary as well, or they may be located symmetrically with respect to the imaginary axis. (In the next section, we shall conjecture that the optimal configuration occurs when this pair of roots coalesces into a double root on the imaginary axis.)

Turning to (3.8), one notices that it is a quartic equation with real coefficients that is missing its cubic term. The typical configuration of roots is therefore one in each quadrant of the complex θ -plane, at equal distances from the real axis. The exception is when (3.8) admits four real roots, which would mean saddle points on the imaginary θ -axis. Considering the minus sign in (3.8) we see this cannot happen when $mn < 2$, and because of (3.10) below, we disregard this possibility.

Figure 3.1 shows a typical configuration of critical and saddle points. The roots of (3.6) are represented by +’s and ×’s (corresponding to the + and – signs, respectively), and the roots of (3.7) are plotted as the *’s.

We propose a saddle point analysis based on the contours shown in the figure. The Γ_{\pm} are the curves of steepest descent $\text{Im}\{g_{\pm}(\theta)\} = \text{constant}$. Writing $\theta = x + yi$, they can be expressed as

$$\Gamma_{\pm} : \frac{4m\pi^2xy}{(x^2 - y^2 - \pi^2)^2 + 4x^2y^2} - (mn \pm 2)x = c_{\pm}.$$

The constants c_{\pm} are determined by the requirement that each Γ_{\pm} passes through its corresponding saddle point, θ_+ or θ_- , as defined by (3.6).

In the lower half-plane, Γ_- starts at $\theta = -\pi$, passes through θ_- , and continues to $\theta = -i\infty$. This is valid since the integrand in (3.5), with minus sign, approaches zero as $\theta \rightarrow -i\infty$, provided that

$$(3.10) \quad mn < 2.$$

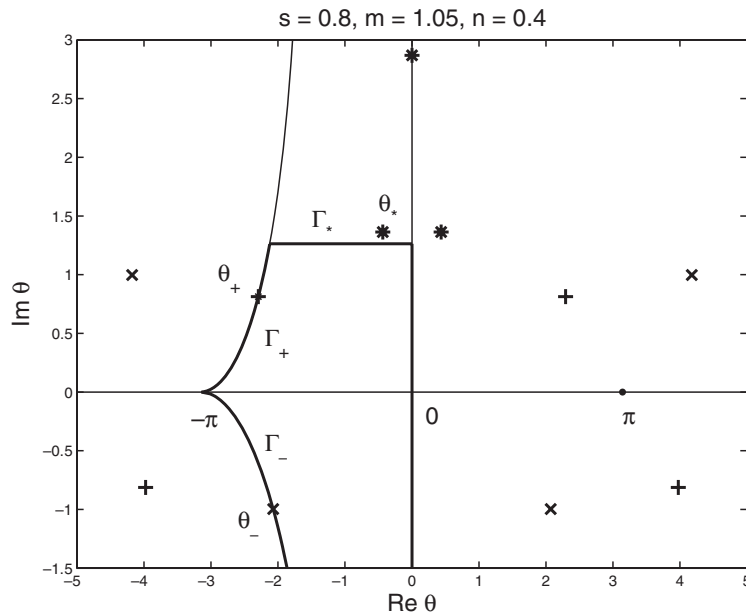


FIG. 3.1. Saddle points, θ_- and θ_+ , critical points θ_* , and steepest descent contours used in deriving the error estimates (3.11)–(3.13).

(The corresponding restriction for the contour (1.3) is $m(1 + n) < 2$.) The contour is then closed at $-i\infty$ and returns to the origin via the negative imaginary θ -axis. On this axis the contribution can be ignored, since the integrand is real. The error $E_N^-(t)$ is therefore solely determined by the saddle point contribution, which can be computed in the usual manner as [1, sect. 6.4; 3, sect. 6.6]

$$(3.11) \quad E_N^-(t) = O(e^{d_- N}), \quad d_- = \text{Re}\{g_-(\theta_-)\}.$$

In the upper half-plane a similar approach is used, except for the fact that the critical points θ_* have to be taken into account. The contour Γ_+ is not continued to $\theta = +i\infty$, as it will not be possible to return to the origin without crossing the singular points $\theta = \theta_*$. To maintain analyticity of the integrand, we introduce a third contour, Γ_* , that branches off from Γ_+ and has a constant imaginary part, say $\text{Im}\{\Gamma_*\} = b$. Typically, the value of b would be determined by the critical point θ_* nearest to the real axis. By letting Γ_* approach such a limiting θ_* from below, it is possible to establish

$$(3.12) \quad E_N^+(t) = O(e^{d_* N}), \quad d_* = \text{Re}\{g_+(\theta_*)\}.$$

If θ_+ lies below Γ_* , a saddle point contribution similar to (3.11),

$$(3.13) \quad E_N^+(t) = O(e^{d_+ N}), \quad d_+ = \text{Re}\{g_+(\theta_+)\},$$

is to be added to (3.12).

In our numerical experiments, the total error was dominated either by (3.11) or by (3.12). We have not found a set of parameters (s, m, n) for which (3.13) dominates, but neither have we tried to prove that this is impossible.

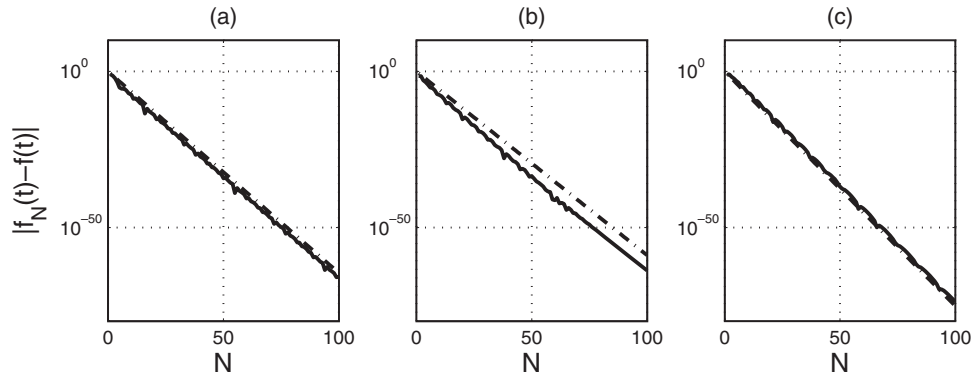


FIG. 3.2. Convergence curves for Talbot's method applied to the model problem (1.10), with $\lambda = -1$, $t = 1$, and using contour (1.5). The solid curves represent the actual errors, and the dash-dot lines (virtually indistinguishable in (a) and (c)) their theoretical estimates. The plots (a)–(c) correspond to three different choices of (s, m, n) , as summarized in the appendix.

In Figure 3.2, we offer numerical verification of these error estimates. In the appendix, the corresponding values of saddle points, critical points, and expected convergence rates are summarized. We have picked sets of parameter values (s, m, n) for which (a) the saddle point contribution (3.11) dominates, (b) the critical point contribution (3.12) dominates, and (c) these two contributions are equal (the conjectured optimal situation). Also shown, as the dash-dot curves, are the predicted convergence rates, i.e., the maximum of (3.11) and (3.12). Here we should point out that these estimates are asymptotic, and much information is suppressed by the order notation of (3.11)–(3.13). Therefore, in some cases N has to be large for the estimate to become valid. This can be seen in part (b) of Figure 3.2, for example, where N has to be greater than 70, roughly, before (3.12) becomes evident.

In Figure 3.2, and elsewhere in the paper where multiprecision arithmetic was required, we computed in Maple and exported the numbers to MATLAB for plotting.

4. Computing the optimal parameters. A first attempt at finding optimal parameters (s, m, n) was based on a numerical optimization strategy, involving the objective function

$$(4.1) \quad F(s, m, n) \equiv \max \{d_+, d_-, d_*\} = \text{minimum}.$$

Here d_+, d_-, d_* are the decay constants in the error estimates (3.13), (3.11), and (3.12). For each set of parameters (s, m, n) , the value of F can be computed by first solving (3.6) and (3.7) to obtain θ_+, θ_- , and θ_* . These values are then substituted into $g_{\pm}(\theta)$, to compute d_+, d_-, d_* as defined by (3.11)–(3.13).

In the case of contour (1.5), (3.6) and (3.7) can be solved with polynomial rootfinding routines, and in this case MATLAB's function `roots` was used. In the case of contour (1.3) a complex Newton process was used. When solving (3.7), one should take care to select the correct root θ_* .

The problem (4.1) was solved using MATLAB's function `fminsearch`, a routine suitable for nonsmooth, unconstrained optimization. Aside from some mild ill-conditioning that will be explained below, this approach worked well.

In the case of contour (1.5), this yielded the parameters presented as case (c) in Figure 3.2, namely

$$(4.2) \quad s = 0.7556, \quad m = 0.8597, \quad n = 0.3029.$$

The corresponding saddle and critical points are summarized in the appendix. The predicted optimal convergence rate is

$$(4.3) \quad E_N(t) = O(e^{-1.7303N}), \quad N \rightarrow \infty.$$

Applying the same algorithm to the original Talbot contour (1.3), we obtained a better convergence rate, namely

$$(4.4) \quad E_N(t) = O(e^{-1.8975N}), \quad N \rightarrow \infty.$$

This corresponds to parameter values

$$(4.5) \quad s = 0.4814, \quad m = 0.6443, \quad n = 0.5653,$$

with saddle points and critical point given by

$$(4.6) \quad \theta_+ = -2.5293 + 0.7435i, \quad \theta_- = -2.4158 - 0.9487i, \quad \theta_* = 0.9487i,$$

and decay rates

$$d_+ = -2.5048, \quad d_- = -1.8975, \quad d_* = -1.8975.$$

In Figure 4.1, we show the θ_+ , θ_- , and θ_* defined by (4.6) in the top figure, and their images in the z -plane in the bottom figure. Also shown are the nodes of the midpoint approximation, with $N = 16$.

Examining the numerical results (4.5)–(4.6), we conjecture that in the optimal configuration,

- (a) θ_* is on the positive imaginary axis,
- (b) $\zeta'(\theta_*) = 0$,
- (c) $\text{Im}(\theta_*) = -\text{Im}(\theta_-)$, and
- (d) $d_+ < d_- = d_*$

for both contours (1.3) and (1.5). All of these properties seem plausible, but we have not pursued rigorous proofs.

Property (b) indicates that θ_* is a double root of (3.7), which is the source of the ill-conditioning mentioned at the beginning of the section. Fortunately, assuming properties (a)–(d) to be true, the problem can be reformulated such that it becomes explicitly solvable. The details are as follows.

Using properties (a) and (c) above, we write

$$\theta_* = yi, \quad \theta_- = x - yi,$$

where $x < 0$ and $y > 0$. Because of property (d), we shall ignore θ_+ and try to solve for x , y , s , m , and n from the following five (real) equations: the right-hand equality in (3.6) (two real equations), (3.7), property (b), and the equality in (d).

Using a straightforward but tedious hand calculation this 5×5 system was reduced to a 2×2 system involving x and y . In the case of contour (1.5) this system is

$$(4.7) \quad \begin{aligned} x(P^2 - Q^2) + 2yPQ &= 0, \\ (5y^2 + \pi^2)(P^2 + Q^2) + P(y^2 + \pi^2)^2 &= 0, \end{aligned}$$

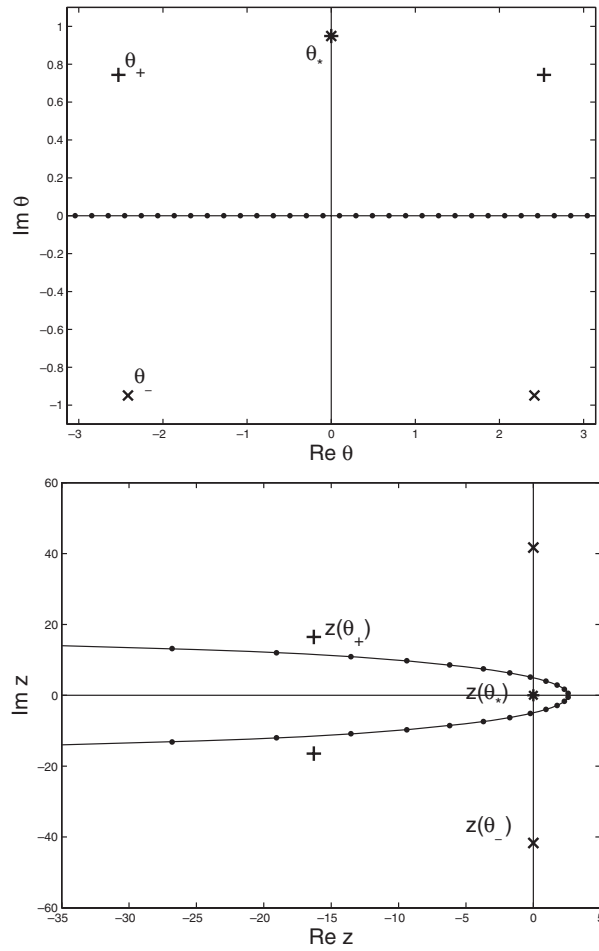


FIG. 4.1. The optimal configuration of saddle points and critical points in the θ -plane (top) as well as their images in the z -plane (bottom). The dots are the nodes used in the midpoint rule, with $N = 16$. Note that in the bottom figure, four sets of nodes lie offscale (towards $Re z = -\infty$). The contour is given by (1.3), but the figure is qualitatively similar for (1.5).

where

$$P = x^2 - y^2 - \pi^2, \quad Q = 2xy.$$

For further simplification we turned to Maple, which produced an explicit solution

$$y = \pi\sqrt{v},$$

where $v \approx 0.07584$ is the smallest positive root of

$$41v^4 - 308v^3 - 98v^2 - 4v + 1 = 0.$$

With this value of v , x is given by

$$x = -\frac{\pi}{4\sqrt{2}}\sqrt{41 - 209v - 1581v^2 + 205v^3}.$$

These formulas yield the values $y \approx 0.8652$ and $x \approx -2.2315$, as obtained above. The values of s , m , and n given in (4.2) follow from

$$n = \frac{4\pi^2 y}{(y^2 + \pi^2)^2}, \quad m = \frac{2(R^2 + S^2)}{4\pi^2(yR - xS) + n(R^2 + S^2)}, \quad s = m \left(\frac{3y^4 + \pi^4}{(y^2 + \pi^2)^2} \right),$$

where

$$R = P^2 - Q^2, \quad S = 2PQ.$$

In the case of contour (1.3) the analogue of the system (4.7) is

$$\begin{aligned} A - x(A^2 - B^2 + 1) - 2yAB &= 0, \\ xA + yB + y(\coth y - 2y \operatorname{csch}^2 y) &= 0, \end{aligned}$$

where we have defined $A = \operatorname{Re}\{\cot \theta_-\}$, $B = \operatorname{Im}\{\cot \theta_-\}$, i.e.,

$$A = \frac{\sin x \cos x}{\sin^2 x + \sinh^2 y}, \quad B = \frac{\sinh y \cosh y}{\sin^2 x + \sinh^2 y}.$$

A numerical solution of this system yields the value of $\theta_- = x - iy$ reported in (4.6). The values of the other parameters can be computed via

$$n = \coth y - y \operatorname{csch}^2 y, \quad m = \frac{2}{B + y(A^2 - B^2 + 1) - 2xAB + n}, \quad s = my^2 \operatorname{csch}^2 y.$$

As verification that the parameters derived here are indeed close to optimal, we offer Figure 4.2. There we show, as the thicker curve, the numerically computed error $E_N(t)$ as a function of N , corresponding to parameters (4.5). Virtually on top of this curve and shown as a dash-dot line is the theoretical error estimate (4.4). To show the near-optimality of these curves, we have computed errors using a uniform sampling of parameter space $(s, m, n) \in (0, 1) \times (0, 1) \times (0, 1)$, with step-size 0.05 in each direction. (That is, $19^3 = 6859$ different parameter sets were used for each value of N .) The vertical line segments in the figure represent the range of these computed errors, with the minima and maxima indicated by the tiny horizontal bars.

We should not neglect to point out that if our sampling of parameter space were finer, some of the lower error bars in this figure could extend further down to 0. This will happen when the two error components, $E_N^+(t)$ and $E_N^-(t)$ in (2.4), are approximately of equal magnitude but of opposite sign. Such instances of fortuitous cancellation will, however, be rare when the matrix as opposed to the scalar problem is solved. We believe that Figure 4.2 represents solid evidence that the suggested parameter values in (4.5) and (4.2) are indeed asymptotically optimal.

To conclude this section, we point out a redundancy in the Talbot contour as noted by Trefethen [21]. Recall Figure 4.1, where the optimal Talbot contour was shown for the case $N = 16$, and recall also that four pairs of nodes were located outside the frame of the figure, towards $\operatorname{Re} z = -\infty$. In fact, the contribution of each of these outlying nodes is negligible, as $|e^{z(\theta_k)t}| \leq e^{-1.90N}$ when $|k| \geq 3N/4$. It appears that practically no accuracy is lost by including only the middle 75% of nodes and discarding the outlying 25%. A more careful calculation shows that the actual fraction of nodes retained should be about 0.7409. Since $1.8975/0.7409 \approx 2.5611$, the effective convergence rate improves from about $O(e^{-1.90N})$ to $O(e^{-2.56N})$. In the case of the modified Talbot contour (1.5) about 28% of the nodes can be discarded, which increases the effective rate from $O(e^{-1.73N})$ to roughly $O(e^{-2.41N})$.

In the next section we solve two parabolic problems to test some of these convergence estimates.

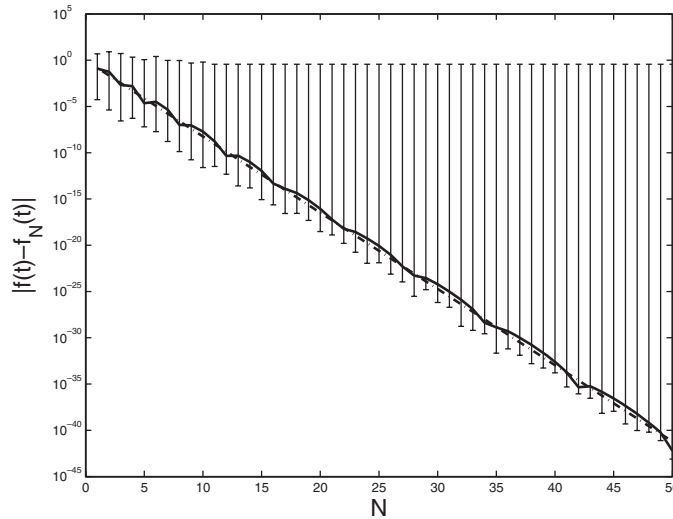


FIG. 4.2. Absolute errors when Talbot's method is applied to the model function (1.10), with $t = 1, \lambda = -1$, using the original contour (1.3). (The figure is qualitatively similar for the modified contour (1.5).) The thicker curve represents the errors computed with the optimal parameters (4.5). The dash-dot line (hardly visible) represents the theoretical error estimate (4.4). The vertical line segments represent the range of errors computed in a uniform sampling of parameter space.

5. Application to PDEs. The prototype parabolic PDE is the heat equation

$$(5.1) \quad u_t = u_{xx}, \quad 0 \leq x \leq \pi,$$

and here we consider boundary conditions

$$(5.2) \quad u(0, t) = 0, \quad u(\pi, t) = 1, \quad t > 0,$$

and an initial condition

$$(5.3) \quad u(x, 0) = 0, \quad 0 \leq x \leq \pi.$$

The exact solution can be represented either as a Fourier series [2, p. 91], or an infinite series involving the complementary error function [2, p. 93] (efficient for large and small t , respectively).

For numerical work, we let $v(x, t) = u(x, t) - x/\pi$ and rewrite the PDE as

$$(5.4) \quad v_t = v_{xx},$$

now with homogeneous boundary conditions

$$(5.5) \quad v(0, t) = 0, \quad v(\pi, t) = 0, \quad t > 0,$$

but inhomogeneous initial condition

$$v(x, 0) = -x/\pi, \quad 0 \leq x \leq \pi.$$

To semidiscretize (5.4), a suitable partition $\{x_j\}_{j=1}^M$ of $[0, \pi]$ is introduced, along with an $M \times M$ matrix D that represents the approximation to d^2/dx^2 and which

incorporates the boundary conditions (5.5). The approximation to (5.1) is then given by the linear system of ODEs

$$(5.6) \quad \mathbf{v}_t = D\mathbf{v}, \quad \mathbf{v}(0) = \mathbf{v}_0.$$

Here $\mathbf{v} = \mathbf{v}(t)$ is the $M \times 1$ column vector $[v_1(t), v_2(t), \dots, v_M(t)]^T$, with $v_j(t)$ representing the approximation to $v(x_j, t)$. Likewise \mathbf{v}_0 is the vector consisting of samples of $v(x, 0)$ at the grid-points x_j .

Traditionally, the system (5.6) is integrated by a Runge–Kutta or multistep formula (the method of lines). Here we use the transform approach instead. That is, we compute the midpoint sum

$$(5.7) \quad \mathbf{v}_N(t) = \frac{1}{N} \operatorname{Im} \left\{ \sum_{k=0}^{N-1} e^{z(\theta_k)t} z'(\theta_k) \mathbf{F}_k \right\},$$

where $z(\theta)$ is given by (1.3) and θ_k by (1.7). The vectors \mathbf{F}_k are solved from

$$(5.8) \quad \left(z(\theta_k) I - D \right) \mathbf{F}_k = \mathbf{v}_0, \quad k = 0, \dots, N-1.$$

The details of our particular implementation are as follows. Since we have established that the Talbot contour (1.3) is superior to the contour (1.5), we consider only the former. As for the choice of $\{x_j\}_{j=1}^M$ and D , we use the Chebyshev spectral collocation method; i.e., the nodes are the Chebyshev points of the second kind, and D is the corresponding spectral second derivative matrix incorporating the boundary conditions (5.2). The canonical interval for the Chebyshev points is $[-1, 1]$, which we transform to $[0, \pi]$ with $x \mapsto (\pi/2)(x+1)$. (Codes for computing $\{x_j\}_{j=1}^M$ and D and further details of the spectral method can be found in [7, 20, 25].)

We shall report errors in the L_2 -norm, as approximated by the Clenshaw–Curtis rule (the natural quadrature rule for the Chebyshev method). That is, we define as error norm

$$(5.9) \quad E_N(t) = \sqrt{\frac{\pi}{2} \sum_{j=1}^M w_j \left(v(x_j, t) - v_j(t) \right)^2},$$

where the w_j are the weights defined in [20, p. 128], and the factor $\pi/2$ comes from the transformation of $[-1, 1]$ to $[0, \pi]$. The exact solution, $v(x, t)$, was computed by the series expansions mentioned below (5.3).

Our first aim is to demonstrate that the convergence estimate (4.4), derived for the model problem (2.1), is also valid for the solution of a PDE. In the latter case, there is of course a spectrum of λ 's present, not only the single λ that was assumed in sections 2 and 3. For this reason we chose the side conditions (5.2)–(5.3) to represent a discontinuous solution at $t = 0$. Our interest will therefore be in the regime $t \rightarrow 0$, when high frequency modes are relevant.

In Figure 5.1 we show solutions of (5.1)–(5.3) at various values of t . We also show the error, $E_N(t)$, as a function of N , for the corresponding values of t . We have chosen the $M \times M$ Chebyshev matrices D sufficiently large to fully resolve the solution; i.e., the errors reported in the figure are solely due to the Laplace transform quadrature error and not due to inadequate spatial resolution. Owing to the smoothing property of the heat equation the order of D can of course be reduced as t increases, and suitably large values of M were determined by trial and error.

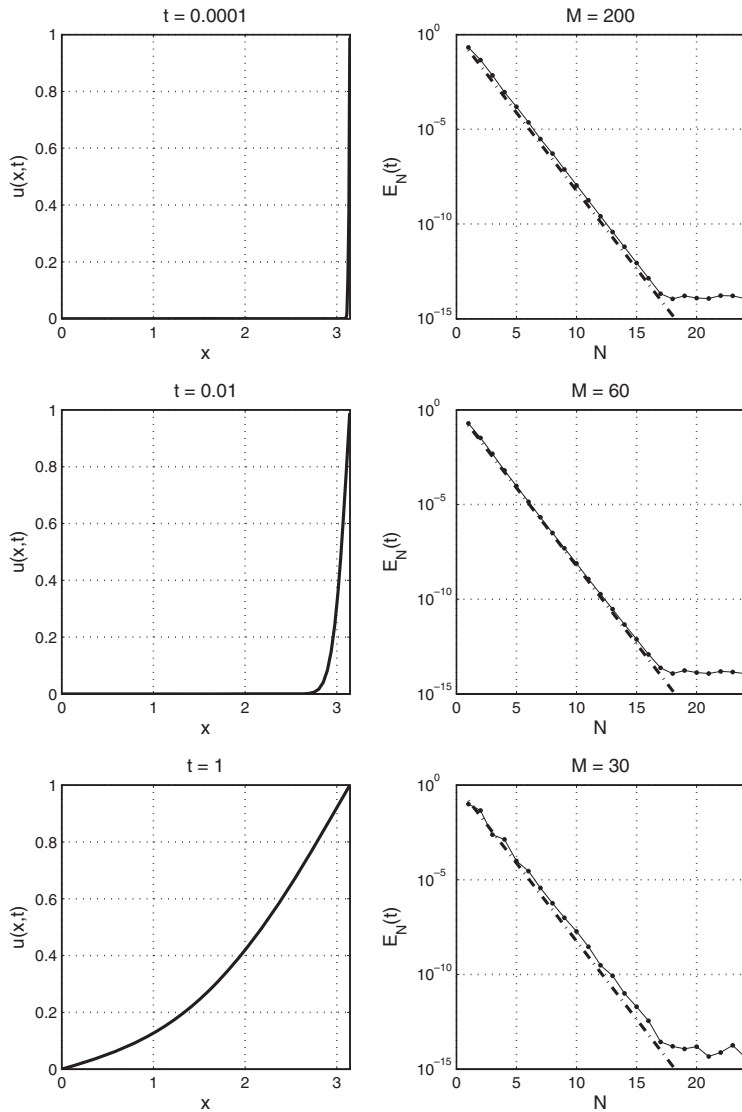


FIG. 5.1. The left column shows the actual solution of (5.1)–(5.3) at various times. The right column shows convergence curves when the solution on the left is approximated with a Chebyshev spectral differentiation matrix of order $M \times M$ and Talbot's quadrature rule (5.7) using the contour (1.3) with optimal parameters (4.5). The thinner, dotted curves show the computed errors, and the thicker, dash-dot lines the error model $\exp(-1.90N)$; cf. (4.4). The error $E_N(t)$ is defined by (5.9).

Assessing these figures, it is clear that the error estimate (4.4) is valid for this problem, even for small t . In addition, one should keep in mind that these results can be achieved by solving effectively only $0.74N$ linear systems (recall the discussion at the end of section 4). This allows us to formulate the rule of thumb stated in the abstract. Suppose an accuracy of $10^{-\ell}$ is required at a particular value of t . By considering

$$e^{-2.56N} = 10^{-\ell} \quad \implies \quad N \approx 0.9\ell$$

one concludes that this should require no more than ℓ solutions of the system (5.8).

We remark that discretization in space is, strictly speaking, not necessary for (5.1)–(5.3), as the Laplace transform can be obtained explicitly, as follows [2, p. 89]:

$$F(z) = \frac{\sinh(x\sqrt{z})}{z \sinh(\pi\sqrt{z})}.$$

Talbot's method (or any other inversion algorithm) may be applied to this transform for any x in $[0, \pi]$. For problems with nonconstant coefficients or with complicated boundary conditions, however, such explicit representations may not exist.

As a second example, we consider the fractional heat equation

$$(5.10) \quad D_t^\alpha u = u_{xx},$$

subject to boundary conditions (5.5) and initial condition

$$(5.11) \quad u(x, 0) = \sin x, \quad 0 \leq x \leq \pi.$$

Here D_t^α is the Caputo fractional derivative, defined by [16, p. 79]

$$D_t^\alpha f(t) = \frac{1}{\Gamma(1-\alpha)} \int_0^t \frac{f'(s)}{(t-s)^\alpha} ds \quad (0 < \alpha < 1).$$

It can be shown [16, p. 79] that if $f(t)$ is twice continuously differentiable, then in the limit $\alpha \rightarrow 1$ this formula reproduces the ordinary derivative, in which case (5.10) reduces to the standard heat equation (5.1).

The analytical solution to (5.10)–(5.11) can be written as

$$u(x, t) = M(t) \sin x,$$

where $M(t)$ can be expressed in terms of the Mittag-Leffler function. In the case $\alpha \rightarrow 1$, it reduces to $M(t) = e^{-t}$. In the case $\alpha = 1/2$, the function can be expressed in terms of the complementary error function, namely

$$M(t) = e^t \operatorname{erfc}(\sqrt{t}).$$

The qualitative properties of this $\alpha = 1/2$ solution are similar to those of the ordinary heat equation, but steady-state is approached on a longer time scale (subdiffusion).

For the numerical solution of (5.10)–(5.11), one takes a Laplace transform of (5.10), which yields

$$\mathbf{F}(z) = (zI - z^{1/2}D)^{-1} \mathbf{u}_0.$$

We shall continue to let D be the Chebyshev second derivative matrix that incorporates the boundary conditions (5.5). The modification to the Talbot method (5.7)–(5.8) is obvious: the scalar $z(\theta_k)^{1/2}$ should be inserted to multiply D in (5.8).

Finding optimal parameters for Talbot's method for the problem (5.10)–(5.11) would mean analyzing $F(z) = 1/(z - z^{1/2}\lambda)$ as a test function. Note that the singularities are no longer isolated, but a branch cut on the negative real axis. Instead of performing such an analysis, we merely demonstrate numerically that Talbot's method with the parameter choices of section 3 is very accurate for this problem as well. The error curves shown in Figure 5.2 confirm that the convergence rate is, to a good approximation, again given by $O(e^{-1.90N})$.

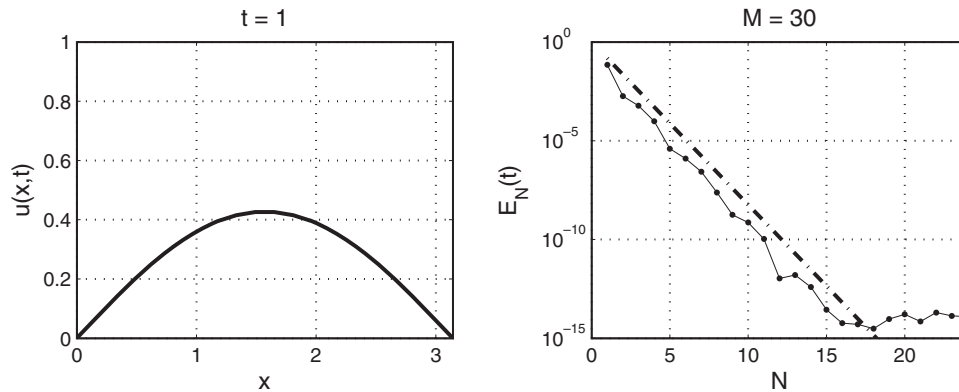


FIG. 5.2. Same as Figure 5.1, but the problem is the fractional PDE (5.10)–(5.11), with $\alpha = 1/2$.

6. Comparisons. Using a combination of asymptotics and heuristics, Talbot made some suggestions for parameter selection in the original paper [19]. In the case of singularities on the real negative axis, the suggested values are

$$\sigma = 0, \quad \mu = \frac{\omega}{t}, \quad \nu = 1.$$

The recommended value of ω is 6 (resp., 11) for single (resp., double) precision. In our notation $\omega = mN$, and using $m = 0.6443$ we find that $\omega = 6$ (resp., 11) corresponds to $N \approx 9$ (resp., 17). This is commensurate with our results, as $\exp(-1.90 \times 9) \approx 3.7 \cdot 10^{-8}$ (approx. single precision) and $\exp(-1.90 \times 17) \approx 9.4 \cdot 10^{-15}$ (approx. double precision). The recommended values $\sigma = 0$ and $\nu = 1$, however, are suboptimal. Indeed, in the abstract of [19] it is stated that “The required number of points depends on t ... and for moderate t is typically 11 for orders of 10^{-6} , 18 for order 10^{-10} , 35 for order 10^{-20} .” Fitting a model $E_N = \text{const.} \times e^{-cN}$ to these data yields $c \approx 1.35$, which is not as good as the $c \approx 1.90$ and $c \approx 2.56$ obtained here.

To be fair to Talbot, the aims of the paper [19] were more ambitious than those of the present paper. To begin with, all singularity distributions were taken into account, not just poles on the negative imaginary axis. In addition, Talbot considered finite precision tolerances, and therefore had to deal with the locations of the singularities. By contrast, we let $N \rightarrow \infty$, thereby making the errors independent of the singularities, and trusted in the power of asymptotics to make the parameters thus found relevant for finite (indeed, relatively small) values of N as well.

More recently, hyperbolic and parabolic contours have been considered as alternatives to Talbot’s contours. Published convergence rates are all subgeometric, namely $O(e^{-cN^{1/2}})$ for the hyperbola of [14], $O(e^{-cN^{2/3}})$ for the parabola of [8], and $O(e^{-cN/\log N})$ for the hyperbola of [12]. The hyperbola has the advantage that it can handle singularities that lie in a sectorial region about the negative real axis; see [12].

Using a rescaling similar to (3.1), the above convergence rates were subsequently improved to the geometric $O(e^{-cN})$; see [13, 26]. In fact, the optimal decay constant c is marginally better for parabolas and hyperbolas than for Talbot contours. With the modification introduced at the end of section 4, however, the Talbot contours regain their superiority.

Appendix. Table A.1 lists saddle points, critical points, and estimated convergence rates corresponding to cases (a)–(c) in Figure 3.2.

TABLE A.1

Case	Parameters	Roots of (3.6)(+)	Roots of (3.6)(-)	Roots of (3.7)	$\theta_+, \theta_-, \theta_*$	d_+, d_-, d_*	Conv. rate
(a)	$s = 0.8$	$\pm 3.9751 - 0.8123i$	$\pm 4.1761 + 0.9975i$	$2.8686i$	$-2.2930 + 0.8123i$	-2.2380	
	$m = 1.05$	$\pm 2.2930 + 0.8123i$	$\pm 2.0710 - 0.9975i$	$\pm 0.4351 + 1.3633i$	$-2.0710 - 0.9975i$	-1.4859	$\exp(-1.4859N)$
	$n = 0.4$				$-0.4351 + 1.3633i$	-2.7267	
(b)	$s = 0.6$	$\pm 3.8710 - 0.7145i$	$\pm 4.0372 + 0.8700i$	$0.6780i$	$-2.4033 + 0.7145i$	-2.1185	
	$m = 0.8$	$\pm 2.4033 + 0.7145i$	$\pm 2.2258 - 0.8700i$	$\pm 1.9043 + 1.9110i$	$-2.2258 - 0.8700i$	-1.4908	
	$n = 0.5$				$0.6780i$	-1.3560	$\exp(-1.3560N)$
(c)	$s = 0.7556$	$\pm 3.9213 - 0.7620i$	$\pm 4.0319 + 0.8652i$	$5.2713i$	$-2.3503 + 0.7620i$	-2.1524	
	$m = 0.8597$	$\pm 2.3503 + 0.7620i$	$\pm 2.2315 - 0.8652i$	$0.8652i$	$-2.2315 - 0.8652i$	-1.7303	$\exp(-1.7303N)$
	$n = 0.3029$			$0.8652i$	$0.8652i$	-1.7303	

Acknowledgments. Kevin Burrage, Nick Gould, Thomas Schmelzer, and Nick Trefethen all contributed useful suggestions, as did the anonymous referees. The author and Fusen Lin had many discussions on Talbot's method while preparing the thesis [11].

REFERENCES

- [1] M. J. ABLOWITZ AND A. S. FOKAS, *Complex Variables: Introduction and Applications*, 2nd ed., Cambridge University Press, Cambridge, UK, 2003.
- [2] M. Y. ANTIMIROV, A. A. KOLYSHKIN, AND R. VAILLANCOURT, *Applied Integral Transforms*, AMS, Providence, RI, 1993.
- [3] C. M. BENDER AND S. A. ORSZAG, *Advanced Mathematical Methods for Scientists and Engineers*, McGraw-Hill, New York, 1978.
- [4] E. CUESTA AND C. PALENCIA, *A numerical method for an integro-differential equation with memory in Banach spaces: Qualitative properties*, SIAM J. Numer. Anal., 41 (2003), pp. 1232–1241.
- [5] P. J. DAVIS, *On the numerical integration of periodic analytic functions*, in On Numerical Approximation (Proceedings of a Symposium, Madison, WI, 1958), R. E. Langer, ed., The University of Wisconsin Press, Madison, WI, 1959.
- [6] D. G. DUFFY, *On the numerical inversion of Laplace transforms: Comparison of three new methods on characteristic problems from applications*, ACM Trans. Math. Software, 19 (1993), pp. 333–359.
- [7] B. FORNBERG, *A Practical Guide to Pseudospectral Methods*, Cambridge University Press, Cambridge, UK, 1996.
- [8] I. P. GAVRILYUK AND V. L. MAKAROV, *Exponentially convergent parallel discretization methods for the first order evolution equations*, Comput. Methods Appl. Math., 1 (2001), pp. 333–355.
- [9] G. H. GOLUB AND C. F. VAN LOAN, *Matrix Computations*, 3rd ed., The Johns Hopkins University Press, Baltimore, MD, 1996.
- [10] E. T. GOODWIN, *The evaluation of integrals of the form $\int_{-\infty}^{\infty} f(x)e^{-x^2} dx$* , Proc. Cambridge Philos. Soc., 45 (1949), pp. 241–245.
- [11] F. LIN, *Numerical Inversion of Laplace Transforms by Trapezoidal-Type Methods*, Ph.D. dissertation, Oregon State University, Corvallis, OR, 2003.
- [12] M. LÓPEZ-FERNÁNDEZ AND C. PALENCIA, *On the numerical inversion of the Laplace transform of certain holomorphic mappings*, Appl. Numer. Math., 51 (2004), pp. 289–303.
- [13] M. LÓPEZ-FERNÁNDEZ, C. PALENCIA, AND A. SCHÄDLE, *A spectral order method for inverting sectorial Laplace transforms*, SIAM J. Numer. Anal., 44 (2006), pp. 1332–1350.
- [14] W. MCLEAN AND V. THOMÉE, *Time discretization of an evolution equation via Laplace transforms*, IMA J. Numer. Anal., 24 (2004), pp. 439–463.
- [15] C. MOLER AND C. VAN LOAN, *Nineteen dubious ways to compute the exponential of a matrix, twenty-five years later*, SIAM Rev., 45 (2003), pp. 3–49.
- [16] I. PODLUBNY, *Fractional Differential Equations*, Academic Press, San Diego, CA, 1999.
- [17] D. SHEEN, I. H. SLOAN, AND V. THOMÉE, *A parallel method for time-discretization of parabolic problems based on contour integral representation and quadrature*, Math. Comp., 69 (2000), pp. 177–195.
- [18] D. SHEEN, I. H. SLOAN, AND V. THOMÉE, *A parallel method for time discretization of parabolic equations based on Laplace transformation and quadrature*, IMA J. Numer. Anal., 23 (2003), pp. 269–299.
- [19] A. TALBOT, *The accurate numerical inversion of Laplace transforms*, J. Inst. Math. Appl., 23 (1979), pp. 97–120.
- [20] L. N. TREFETHEN, *Spectral Methods in MATLAB*, Software Environ. Tools 10, SIAM, Philadelphia, 2000.
- [21] L. N. TREFETHEN, *private communication*, Oxford University Computing Laboratory, Oxford, UK, 2005.
- [22] A. M. TURING, *A method for the calculation of the zeta-function*, Proc. London Math. Soc. (2), 48 (1943), pp. 180–197.
- [23] J. A. C. WEIDEMAN, *Numerical integration of periodic functions: A few examples*, Amer. Math. Monthly, 109 (2002), pp. 21–36.

- [24] J. A. C. WEIDEMAN, *Optimizing Talbot's Contours for the Inversion of the Laplace Transform*, Technical report NA 05/05, Oxford University Computing Laboratory, Oxford, UK, 2005.
- [25] J. A. C. WEIDEMAN AND S. C. REDDY, *A MATLAB differentiation matrix suite*, ACM Trans. Math. Software, 26 (2000), pp. 465–519.
- [26] J. A. C. WEIDEMAN AND L. N. TREFETHEN, *Parabolic and hyperbolic contours for computing the Bromwich integral*, Math. Comp., to appear.